PHYSICAL REVIEW B **83**, 180401(R) (2011)

Magnetic dynamics driven by the spin current generated via the spin Seebeck effect

Chenglong Jia[1,2] and Jamal Berakdar[1]

[1]*Institut für Physik, Martin-Luther Universität Halle-Wittenberg, D-06099 Halle, Germany*

[2]*Key Laboratory for Magnetism and Magnetic Materials of the Ministry of Education, Lanzhou University, Lanzhou 730000, China*

(Received 8 February 2011; revised manuscript received 2 March 2011; published 2 May 2011)

We consider the spin-current-driven dynamics of a magnetic nanostructure in a conductive magnetic wire under a heat gradient in an open-circuit, spin-Seebeck-effect geometry. It is shown that the spin-current scattering results in a spin-current torque acting on the nanostructure and leading to precession and displacement. The scattering leads also to a redistribution of the spin electrochemical potential along the wire, resulting in a break of the polarity-reversal symmetry of the inverse spin Hall effect voltage with respect to the heat-gradient inversion.

DOI: 10.1103/PhysRevB.83.180401 PACS number(s): 75.30.Hx, 85.75.−d, 72.25.Pn, 85.80.−b

Introduction. The discovery in the 1820s by Seebeck that due to a temperature gradient, an electric voltage emerges along the temperature drop, revealed the relationship between heat and charge currents. The reversal of Seebeck's effect, i.e., the appearance of a temperature gradient upon an applied voltage, was shortly thereafter confirmed by Peltier in 1834. In addition to other thermo-electric phenomena such as Joule heating, in magnetic fields, new thermomagnetic effects arise: A resistive conductor with a temperature gradient ∇T placed in a magnetic field $\mathbf{B}$ perpendicular to ∇T develops a potential drop normal to both ∇T and $\mathbf{B}$. This phenomenon is termed the Ettingshausen effect, and its reverse is the Nernst effect. In a magnetic material, the anomalous Nernst effect occurs (due to the spontaneous magnetization), which was first observed for Ni and Ni-Cu alloy.[1,2] Recently, in Refs. 3–6, measurements of the planar and the anomalous Nernst effect were reported for a variety of materials, including magnetic semiconductors, ferromagnetic metals, pure transition metals, oxides, and chalcogenides. A qualitatively new phenomena, the spin Seebeck effect (SSE), was reported in 2008 by Uchida *et al.*,[7] showing that in a ferromagnetic material (a mm-size $Ni_{81}Fe_{19}$ sample) and in an open-circuit geometry (which is also the geometry studied in this work; cf. Fig. 1), a heat current results in a spin current, i.e., a flow of spin angular momentum and hence a spin voltage, even if ∇T is parallel to $\mathbf{B}$ (where the Nernst-Ettingshausen effect does not contribute). The spin voltage is reflected by a charge voltage that emerges [due to the inverse spin Hall effect (ISHE)] in a Pt strip deposited on the sample perpendicular to ∇T (cf. Fig. 1). Further experiments on resistive conductors (see Ref. 8 for $Ni_{81}Fe_{19}$), insulating ferrimagnets ($LaY_2Fe_5O_{12}$ in Ref. 9), and ferromagnetic semiconductors (GaMnAs in Ref. 10) underline the generality of the SSE. These fascinating effects are not only of fundamental importance; thermo-electric elements are already indispensable for temperature sensing and control and for current-heat conversion. The SSE opens the way for thermo-electric spintronic devices with qualitatively new tools for energy-consumption reduction. It is highly desirable to explore whether the SSE can be utilized to steer localized magnetic textures, which is a problem addressed here. Theoretically, the reciprocity between the dynamics in the magnetic order and the heat gradients is governed by the Onsager relations. The Onsager matrix was discussed from a general point of view in Ref. 11, with a focus on the transport of charge, magnetization, and heat.

In Refs. 12 and 13, a thermomagnetic mesoscopic circuit theory was put forward. Reference 14 pointed out the occurrence of a thermally excited spin current in resistive conductors with embedded ferromagnetic nanoclusters. Other recent works[12,13] addressed the thermally induced spin-transfer torque in spin-valve structures, whereas the phenomenological study in Ref. 15 focused on the spin-transfer torques in quasi-one-dimensional magnetic domain walls (DWs) by introducing a viscous term into the Landau-Lifshitz-Gilbert (LLG) equation.

Spin current. The microscopic mechanism for the appearance of the spin current in the SSE is not yet completely understood. It is, however, an experimental fact that in the geometry of Fig. 1, the thermal gradient ∇T generates a steady-state spin current $\mathbf{J}_T^s$ without a charge current.[7–10] The amplitude of $\mathbf{J}_T^s$ is found to be determined by[7–10]

$$\mathbf{J}_T^s = -\kappa \nabla T, \tag{1}$$

where κ is a temperature-independent transport coefficient whose properties are discussed in Refs. 7–10; no charge current is generated. The purpose of this work is to inspect the dynamics triggered by $\mathbf{J}_T^s$ [Eq. (1)] for the case where localized magnetic texture $\mathbf{M}$ (Ref. 16) is present in the ferromagnetic (FM) conductor (cf. Fig. 1), which is a problem of great importance that has not been addressed. As shown below, the quantum-mechanical scattering of $\mathbf{J}_T^s$ from $\mathbf{M}$ acts, in effect, with a spin-current torque on $\mathbf{M}$, which results in an oscillatory and displacement motion of $\mathbf{M}$. Upon scattering, $\mathbf{J}_T^s$ also changes. This leads to a redistribution of the spin electrochemical potential, which can be measured via the ISHE.

The system under consideration is illustrated in Fig. 1. Two thermal reservoirs, with different temperatures T and $T + \Delta T$ in a FM conductive wire of length $2L$, create a steady T gradient ∇T along the x axis, and hence a steady-state spin current $\mathbf{J}_x^s$. This means that without knowing the detail of the operators associated with the SSE, these project the system onto a chargeless eigenstate $\psi(x)$ of the spin-current operator $\hat{\mathbf{j}}_\mu^s(k)$.

Generally, such a state can be written as[19]

$$\psi(x) = \frac{1}{2}\left[e^{ikx}\begin{pmatrix} e^{i\phi} \\ e^{-i\phi}\end{pmatrix} + e^{-ikx}\begin{pmatrix} e^{i\theta} \\ e^{-i\theta}\end{pmatrix}\right]. \tag{2}$$

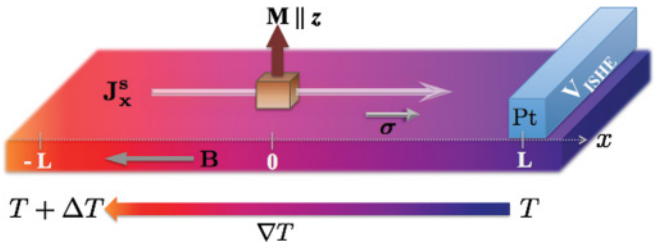

FIG. 1. (Color online) A localized magnetic structure **M** in a ferromagnetic conductor of length $2L$ subject to the constant temperature gradient ∇T. **B** is a saturation magnetic field along ∇T. The pure spin current $\mathbf{J}^s_x$ is signaled by the inverse spin Hall effect voltage $V_{\rm ISHE}$ measured in a Pt strip. The x and z axes are as indicated.

The expectation value x of the charge current $\mathbf{j}^e(k) = \frac{i\hbar}{2m}\{[\nabla\psi^\dagger(x)]\psi(x) - \psi^\dagger(x)\nabla\psi(x)\}$ vanishes, i.e., $j^e_x(k) \equiv 0$ (here m is the effective mass). In contrast, for the spin current $\mathbf{j}^s_\mu(k) = \frac{i\hbar}{2m}\{[\nabla\psi^\dagger(x)]\sigma_\mu\psi(x) - \psi^\dagger(x)\sigma_\mu\nabla\psi(x)\}$, we infer

$$j^s_x(k) = \tfrac{\hbar k}{2m}(\cos 2\phi - \cos 2\theta), \tag{3}$$

$$j^s_y(k) = \tfrac{\hbar k}{2m}(\sin 2\theta - \sin 2\phi). \tag{4}$$

In general, the thermal transport is ballistic,[20] but with diffusive spins, i.e., upon creating Eq. (2), the spin coherence is lifted by scattering events that randomize ϕ and θ within $[0,2\pi]$. Hence, the expectation value of the spin current vanishes on the scale of the spin-flip diffusion length,[21,22] i.e., $\mathbf{J}^s_\mu(k) = \oint \mathbf{j}^s_\mu d\theta d\phi/(2\pi)^2 = 0$. However, when the wire is magnetically polarized and driven to saturation by the magnetic field **B**,[7–10] we find that $\langle\sigma_x\rangle \neq 0$, but $\langle\sigma_y\rangle = 0$. Equation (2) reads then for an exchange-split conductor,

$$\psi_B(x) = \frac{1}{2}\left[e^{ikx}\begin{pmatrix}1\\1\end{pmatrix} + e^{-ikx}\begin{pmatrix}e^{i\theta}\\e^{-i\theta}\end{pmatrix}\right]. \tag{5}$$

Here, $\theta \in [0,2\pi]$ still appears due to the residual spin precession and diffusion. Then we have $J^e \equiv 0$ and $J^s_y(k) = \oint j^s_y d\theta/2\pi = 0$, whereas $J^s_x(k) = J^s_0(k) = \hbar k/2m$, which is in line with the experimental observation.[7–10]

The main purpose of the present work is to investigate the influence of a localized, magnetic, nondiffusive scatterer **M** [where $x = 0$ is taken as its central position (see Fig. 1)]. **M** has a uniaxial anisotropy along an axis chosen to be z. If $\mathbf{M}(x)$ has an internal structure, e.g., a noncollinearity, that varies on a scale larger than $\lambda = 2\pi/k$ [the variation scale of (5)], one can unitarily transform to align locally with **M**, which introduces a weak gauge potential that can be dealt with[23] in a perturbative way using the Green's function constructed from (5) (as similarly done in Refs. 24 and 25). We find that **M** has a stronger influence if its range of variation is comparable to λ. In this case, the magnetic texture acts in effect as $\mathbf{M}(x) = \mathbf{M}_0\delta(x)$, where the magnetic moment $\mathbf{M}_0$ derives from an average of $\mathbf{M}(x)$ over its extension w. The model is realizable for Ref. 10 rather than for metals. The interaction between **M** and the electron spin $\boldsymbol{\sigma}$ reads[26]

$$H_{\rm int} = g\mathbf{M}(x)\cdot\boldsymbol{\sigma}, \tag{6}$$

where g is a local coupling constant and M_0 is large enough to be treated classically. For $\mathbf{M}_0$ aligned with the z axis, as in Fig. 1, we derive, using Eqs. (5) and (6), the expression for the spinor wave function in the presence of $\mathbf{M}(x)$, namely

$$\psi_s(x) = \begin{cases} \frac{e^{ikx}}{2}\binom{1}{1} + \frac{e^{-ikx}}{2}\binom{r}{r^\star} + \frac{e^{-ikx}}{2}\binom{te^{i\theta}}{t^\star e^{-i\theta}} & \text{for } x < 0, \\ \frac{e^{-ikx}}{2}\binom{e^{i\theta}}{e^{-i\theta}} + \frac{e^{ikx}}{2}\binom{re^{i\theta}}{r^\star e^{-i\theta}} + \frac{e^{ikx}}{2}\binom{t}{t^\star} & \text{for } x > 0. \end{cases} \tag{7}$$

The scattering state $\psi_s(x)$ describes the spinor wave function in the original-spin channel, which is partially reflected into the original-spin and the spin-flip channels, and also partially transmitted into these two channels, which gives the complex spin reflection and transmission coefficients r and t,

$$r = -\frac{i\alpha}{1+i\alpha}, \quad t = \frac{1}{1+i\alpha}, \quad \text{where } \alpha = gM_0m/k\hbar^2. \tag{8}$$

The magnetic scattering gives rise to a short pseudocircuit to the charge channels, as we find

$$j^e_x = \frac{2\alpha\sin\theta}{1+\alpha^2}. \tag{9}$$

However, $\langle j^e_x\rangle$ vanishes beyond the spin-diffusion length after averaging over θ. Counterparts, i.e., a pure spin current generated by a charge current when scattered off a magnetic structure, are well known, e.g., see Refs. 26–28. The spin current carried by (5) is modified upon scattering, and a nonzero J^s_y emerges as

$$J^s_x/J^s_0 = \begin{cases} \frac{1+3\alpha^2}{(1+\alpha^2)^2} & \text{for } x < 0, \\ \frac{1-\alpha^2}{(1+\alpha^2)^2} & \text{for } x > 0, \end{cases} \tag{10}$$

$$J^s_y/J^s_0 = \begin{cases} \frac{2\alpha^3}{(1+\alpha^2)^2} & \text{for } x < 0, \\ \frac{2\alpha}{(1+\alpha^2)^2} & \text{for } x < 0. \end{cases} \tag{11}$$

Within the linear response, the spin voltage along the wire is $\mu_s(x) = \xi_s x\langle J^s_x(\alpha)\rangle$, where ξ_s is a function of the elementary charge, the spin-dependent electric conductivity, the spin-dependent Seebeck coefficient, and the spin Seebeck coefficient of the FM wire.[29] The quantum-mechanically averaged spin current is $\langle J^s_x(\alpha)\rangle = {\rm Tr}[J^s_x(\alpha)\rho]$.[30] The single-electron density matrix is $\rho = -\frac{1}{\pi}{\rm Im}\sum_{\mathbf{k}}\frac{\psi_s\psi_s^\dagger}{E_F - E_{\mathbf{k}} + i\Gamma}$, where E_F is the Fermi energy, $E_{\mathbf{k}} = \hbar^2k^2/2m + \hbar^2\mathbf{k}^2_\parallel/2m$ with $\mathbf{k}_\parallel$ being the transverse wave vector, and Γ is a Lorenzian relaxation rate due to disorder.[31] Depositing a conductive strip with a strong spin-orbit coupling, e.g., Pt, as shown in Fig. 1, $\mu_s(x)$ can be imaged via the electric voltage $V_{\rm ISHE}$ generated by the inverse spin Hall effect in Pt using the relation

$$\frac{{\rm V}_{\rm ISHE}(x)}{{\rm V}^0_{\rm ISHE}(L)} = \frac{\langle J^s_x(\alpha)\rangle}{\langle J^s_x(0)\rangle}\frac{x}{L}, \tag{12}$$

where ${\rm V}^0_{\rm ISHE}(x)$ is the electric voltage measured in Pt in the absence of the magnetic scatterer **M**. Explicitly, ${\rm V}^0_{\rm ISHE}(x) = \gamma\xi_s x\langle J^s_x(0)\rangle$, with γ being a system-dependent parameter[7–10] determined by the spin Hall angle in Pt, the spin-injection efficiency across the FM-Pt interface, and the length and thickness of the Pt wire. Due to the spin current scattering off **M**, the Hall voltage ${\rm V}_{\rm ISHE}$ loses its odd symmetry with respect to a reflection at $x = 0$, i.e., we deduce $-{\rm V}_{\rm ISHE}(-x) \neq {\rm V}_{\rm ISHE}(x)$. As shown in Fig. 2, the amount of the symmetry

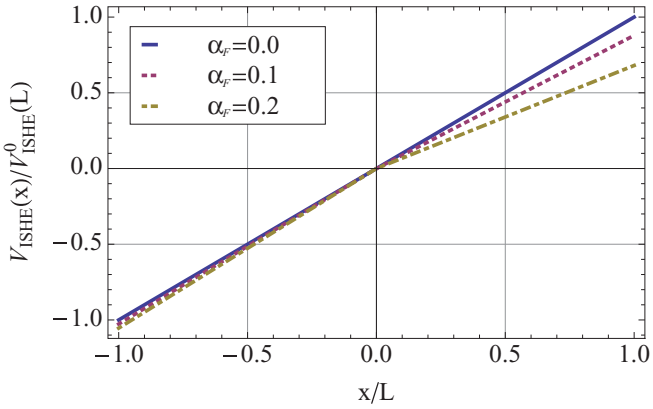

FIG. 2. (Color online) The electric voltage V_{ISHE} generated by the inverse spin Hall effect in the Pt layer as a function of the magnetic scattering strength $\alpha_F = gM_0m/k_F\hbar^2$, with k_F being the Fermi wave vector. The relaxation rate is $\Gamma/E_F = 0.01$.

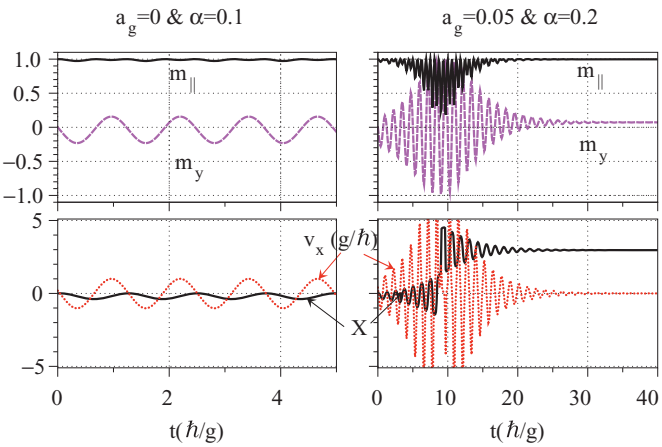

FIG. 3. (Color online) Precession of the magnetic moment **M** [Eq. (16)] for different spin-current scattering strength α [cf. Eq. (8)] and Gilbert damping a_g. Here, $v_x = \partial X/\partial t$ and $D_z/g = 5$.

break depends on α, and can be taken in the experiment as an indicator of the presence of magnetic scattering centers.

Magnetization dynamics. Since J^s_x is modified by the presence of **M**, the scattering triggers a dynamics of **M** which is usually much slower than the carrier scattering dynamics and can be classically treated (M_0 is assumed to be large). J^s_μ acts on **M** with a torque T_μ that follows from the jump in the spin current at the point $x = 0$: $T_\mu = J^s_\mu(0^-) - J^s_\mu(0^+)$. Hence, T_μ derives from our quantum-mechanical calculations as

$$T_x = J^s_0 \frac{4\alpha^2}{(1+\alpha^2)^2}, \quad T_y = -J^s_0 \frac{2\alpha(1-\alpha^2)}{(1+\alpha^2)^2}. \tag{13}$$

Both components are transversal. T_y tends to align **M** to the direction of the FM magnetization, while T_x tries to rotate the moment **M** around the axis $\hat{e}_x$. Equivalently, within our model, the spin-current torque T_μ is obtained from the spin density $S_\mu(x)$ accumulated at the localized moment (due to the interference of incoming and reflected waves) as

$$T_\mu = -\frac{gM_0}{\hbar}[\mathbf{n} \times \mathbf{S}(x=0)], \tag{14}$$

where **n** is the unit vector along **M**, and the spin density is obtained from $S_\mu(x) = \psi^\dagger(x)\sigma_\mu\psi(x)$. Since M_0 is assumed to be large ($\geqslant 5/2\ \mu_B$), the spin-current-induced magnetization dynamics can be treated with the modified LLG equation[32,33]

$$\frac{\partial \mathbf{n}}{\partial t} = \frac{D_z}{\hbar}[\mathbf{n} \times \hat{e}_z] + \frac{a_g}{\hbar}\mathbf{n} \times \frac{\partial \mathbf{n}}{\partial t} - \frac{g}{\hbar}[\mathbf{n} \times \mathbf{S}(0)], \tag{15}$$

where D_z is the anisotropy energy and a_g is the Gilbert damping parameter.[34] Two motion types of **M** occur, precession and displacement, which are discussed below.

Precession. Introducing the following magnetization distribution:

$$\mathbf{n} = [m_\|(t)\sin X(t), m_y(t), m_\|(t)\cos X(t)], \tag{16}$$

and propagating with the LLG equation (15) starting from $m_\|(0) = 1$, $m_y(0) = 0$, and $X(0) = 0$, we calculate the time dependence of **M** shown in Fig. 3. The oscillations of $X(t)$ result in small x and y components of the magnetization. The magnetic moment precesses with a velocity $v_x(t) = \partial X(t)/\partial t$ in the presence of the SSE-generated spin current [$v_x(0) \neq 0$]. We note that the maximum deflection angle X_{max} depends implicitly on the spin-current dynamics through the parameter α, as determined by Eq. (8). Also the Fermi energy enters through the k dependence of α. The dynamics is a mixture of anisotropy-dominated precession and damping.

Displacement. Let us consider the initial localized magnetic-moment distribution,

$$\mathbf{n} = [m_\|(t)\sin\zeta, m_y(t), m_\|(t)\cos\zeta],$$
$$\zeta = \cos^{-1}[\tanh^2(x/w)], \tag{17}$$

where w stands for the extension of the localized moment and $m_\|(0) = 1$, $m_y(0) = 0$, and $x(0) = 0$. As concluded from Fig. 4, the moment is set in motion when subjected to the spin current. The velocity changes from positive to negative, which is different from the motion of a single Néel wall[36] [in which the velocity decreases to zero in a fraction of a nanosecond and the DWs stop completely].

Remarks and conclusions. Our main result is that the SSE-generated spin current in a wire may scatter from a

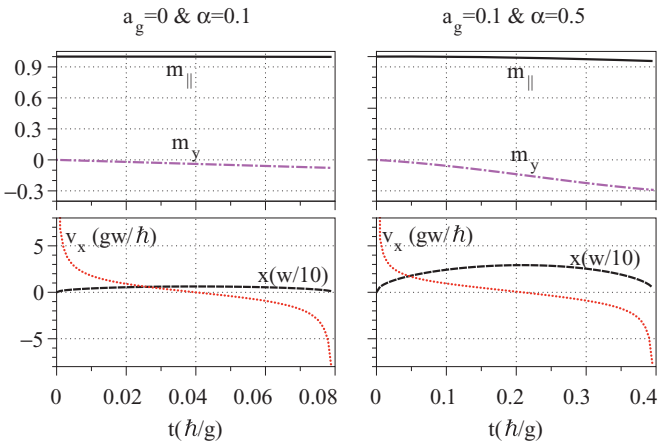

FIG. 4. (Color online) Displacement of the magnetic moment [given by Eq. (17)] vs time for the same parameters of Fig. 3; $v_x = \partial x/\partial t$.

localized magnetic structure, setting it in a precessional and displacement motion. The scattering also leads to a redistribution of the spin current in the wire and hence changes the ISHE signal. From these results, a conclusion can be made regarding the influence of a collection of noninteracting localized moments, but no statement can be made regarding when they interact or even form clusters. We also note that the present conclusions do not apply to a domain wall (DW) [except for a very close, nonresonant (transversal) 180° DW pair, e.g., as in Ref. 37]. In fact, our initial finding[23] is that a single sharp DW is lessaffected by the spin current because the spin-current torques, acting from left and right of the DW, partially compensate. This is not so for an adiabatic or asymmetric DW because the T gradient modifies the DW along ∇T. As for the experimental observation of the magnetic-moment dynamics, it should be noted that the temperature gradient has to be sustained on the time scale of this dynamics; a fast (e.g., femtosecond), strong heat pulse is inappropriate for our (constant ∇T, linear response) study and may cause locally a longitudinal dynamics of **M**.

[1] V. W. Rindner and K. M. Koch, Z. Naturforsch. A **13**, 26 (1958).
[2] G. Nentwich, Z. Naturforsch. A **19**, 1137 (1964).
[3] Y. Onose, Y. Shiomi, and Y. Tokura, Phys. Rev. Lett. **100**, 016601 (2008).
[4] Y. Pu, E. Johnston-Halperin, D. D. Awschalom, and J. Shi, Phys. Rev. Lett. **97**, 036601 (2006).
[5] Y. Pu, D. Chiba, F. Matsukura, H. Ohno, and J. Shi, Phys. Rev. Lett. **101**, 117208 (2008).
[6] T. Miyasato *et al.*, Phys. Rev. Lett. **99**, 086602 (2007).
[7] K. Uchida *et al.*, Nature (London) **455**, 346 (2008).
[8] K. Uchida *et al.*, Solid State Commun. **150**, 524 (2010).
[9] K. Uchida *et al.*, Nature Mater. **9**, 894 (2010).
[10] C. M. Jaworski *et al.*, Nature Mater. **9**, 898 (2010).
[11] M. Johnson and R. H. Silsbee, Phys. Rev. B **35**, 4959 (1987).
[12] M. Hatami, G. E. W. Bauer, Q. Zhang, and P. J. Kelly, Phys. Rev. B **79**, 174426 (2009).
[13] M. Hatami, G. E. W. Bauer, Q. Zhang, and P. J. Kelly, Phys. Rev. Lett. **99**, 066603 (2007).
[14] O. Tsyplyatyev, O. Kashuba, and V. I. Falko, Phys. Rev. B **74**, 132403 (2006).
[15] A. A. Kovalev and Y. Tserkovnyak, e-print arXiv:0906.1002.
[16] As an example, we take a single-molecule magnet Mn_{12} $[Mn_{12}O_{12}(O_2C\text{-}C_6H_4\text{-}SAc)_{16}(H_2O)_4]$ as the local magnetic scatterer **M**. The total spin and diameter of Mn_{12} are $M_0 = 10$ and $w = 3$ nm, respectively.[17] The local exchange coupling between the carriers and the moment **M** is given as $gM_0 = 1$ meV.[18]
[17] H. B. Heersche, Z. de Groot, J. A. Folk, and H. S. J. van der Zant, Phys. Rev. Lett. **96**, 206801 (2006).
[18] R. Q. Wang, L. Sheng, R. Shen, B. Wang, and D. Y. Xing, Phys. Rev. Lett. **105**, 057202 (2010).
[19] We employ a continuous model; a discretized treatment based on Heisenberg spins is straightforward and does not alter qualitatively the amplitude of the spin-charge current.
[20] X. Zotos, F. Naef, and P. Prelovšek, Phys. Rev. B **55**, 11029 (1997); A. V. Sologubenko *et al.*, *ibid.* **62**, R6108 (2000).
[21] M. Hatami, G. E. W. Bauer, S. Takahashi, and S. Maekawa, Solid State Commun. **150**, 480 (2010).
[22] J. Xiao, G. E. W. Bauer, K.-C. Uchida, E. Saitoh, and S. Maekawa, Phys. Rev. B **81**, 214418 (2010).
[23] C. L. Jia and J. Berakdar (unpublished).
[24] N. Sedlmayr, V. K. Dugaev, and J. Berakdar, Phys. Rev. B **79**, 174422 (2009); Phys. Stat. Sol. B **247**, 2603 (2010).
[25] V. K. Dugaev, J. Barnas, and J. Berakdar, J. Phys. A **36**, 9263 (2003).
[26] V. K. Dugaev, V. R. Vieira, P. D. Sacramento, J. Barnaś, M. A. N. Araújo, and J. Berakdar, Phys. Rev. B **74**, 054403 (2006).
[27] A. Vedyayev, M. Chschiev, and B. Dieny, J. Phys. Condens. Matter **20**, 145208 (2008); A. Manchon, N. Ryzhanova, A. Vedyayev, M. Chschiev, and B. Dieny, *ibid.* **20**, 145208 (2008).
[28] M. Araujo, V. Dugaev, V. Veira, J. Berakdar, and J. Barnas, Phys. Rev. B **74**, 224429 (2006).
[29] K. Uchida *et al.*, J. Appl. Phys. **105**, 07C908 (2010).
[30] V. K. Dugaev, J. Berakdar, and J. Barnaś, Phys. Rev. B **68**, 104434 (2003).
[31] O. E. Dial, R. C. Ashoori, L. N. Pfeiffer, and K. W. West, Nature (London) **448**, 176 (2007).
[32] Ya. B. Bazaliy, B. A. Jones, and S.-C. Zhang, Phys. Rev. B **57**, R3213 (1998).
[33] J. Fernández-Rossier, M. Braun, A. S. Núnez, and A. H. MacDonald, Phys. Rev. B **69**, 174412 (2004).
[34] Temperature effects can be included in Eq. (15), as in Ref. 35, by assuming $\boldsymbol{M}$ to be in a local thermal equilibrium at the temperature $T(x = 0)$ (assuming $\nabla T = \text{const}$) and applying the fluctuation-dissipation theorem, which yields a stochastic field that adds to the effective field. In Ref. 35, it is shown that at low T, thermal fluctuations do not alter qualitatively the LLG dynamics.
[35] A. Sukhov and J. Berakdar, Phys. Rev. Lett. **102**, 057204 (2009).
[36] Z. Li and S. Zhang, Phys. Rev. Lett. **92**, 207203 (2004).
[37] V. Dugaev, J. Berakdar, and J. Barnas, Phys. Rev. Lett. **96**, 047208 (2006).